Author Manuscript

Author Manuscript

Author Manuscript

Author Manuscript

HHS Public Access

Author manuscript

ASAIO J. Author manuscript; available in PMC 2018 September 01.

Published in final edited form as:

ASAIO J. 2017 ; 63(5): 637–643. doi:10.1097/MAT.0000000000000616.

A Membrane Lung Design Based on Circular Blood Flow Paths

U. Piyumindri Fernando[*,†], **Alex J. Thompson**[*], **Joseph Potkay**[*], **Hannah Cheriyan**[*], **John Toomasian**[*], **Andreas Kaesler**[‡], **Peter Schlanstein**[‡], **Jutta Arens**[‡], **Ronald B. Hirschl**[*], **Joseph L. Bull**[†], and **Robert H. Bartlett**[*]

[*]Department of Surgery, University of Michigan, Ann Arbor, MI, USA

[†]Department of Biomedical Engineering, University of Michigan, Ann Arbor, MI, USA

[‡]Department of Cardiovascular Engineering, Institute of Applied Medical Engineering, Helmholtz Institute, RWTH Aachen University, Aachen, Germany

Abstract

Current hollow fiber membrane lungs feature a predominantly straight blood path length across the fiber bundle, resulting in limited oxygen transfer efficiency due to the diffusion boundary layer effect. Using computational fluid dynamics and optical flow visualization methods, a hollow fiber membrane lung was designed comprising unique concentric circular blood flow paths connected by gates. The prototype lung, comprising a fiber surface area of 0.28 m^2, has a rated flow of 2 L/min and the oxygenation efficiency is 357 mL/min/m^2. The CO_2 clearance of the lung is 200 mL/min at the rated blood flow. Given its high gas transfer efficiency, as well as its compact size, low priming volume, and propensity for minimal thrombogenicity, this lung design has the potential to be used in a range of acute and chronic respiratory support applications, including providing total respiratory support for infants and small children and CO_2 clearance in adults.

Keywords

Artificial lung; circular flow; mixing; oxygenation

Introduction

In current hollow fiber membrane lungs, the primary blood path is straight flow directed across the fiber bundle from inlet to outlet. Only the red blood cells that are in contact with the gas exchange surface of each fiber are oxygenated; this is known as the boundary layer effect.[1] Mixing of the flowing blood to disrupt the boundary layer is achieved by the small secondary flows induced as the blood contacts each successive fiber.[2] This results in 100–200 mL oxygen exchange per minute per square meter at rated flow.[3] The rated flow is the flow of standardized venous blood that leaves the membrane lung at 95% oxyhemoglobin saturation.

Corresponding Author: Robert H. Bartlett MD, University of Michigan ECLS Laboratory, 1150 W. Medical Center Drive, B560 MSRBII, Ann Arbor, MI 48109, Phone: (734) 615-5357, Fax (734) 615-4220, robbar@umich.edu.

No Conflicts of Interest

Author Manuscript Author Manuscript Author Manuscript Author Manuscript

Years ago we described that the induction of secondary flows in a circular chamber could decrease the boundary layer effect, ultimately reaching the diffusion limit of the PDMS (silicone rubber) membrane.[4–6] Vortices were generated by rapidly moving the membrane surface of the circular chamber against static or slowly flowing blood. A membrane lung using flat sheet PDMS was formed into concentric circular chambers connected by gates, which reached membrane limitation for oxygen diffusion for PDMS. Secondary flows were created by mechanical oscillation of the device. The oxygen transfer efficiency was 205 mL/min/m^2, the limit for a 5 mill PDMS membrane. The fabrication problems and noise made the design impractical for clinical use, but demonstrated that oxygen transfer efficiency is based on the extent of secondary flows.

Similar secondary flows are generated when blood flows through a static circular chamber with a curved flow path.[7,8] The higher the flow, the more intense the secondary flow vortices formed. We hypothesized that: circular blood flow chambers with no corners should minimize thrombosis, a membrane lung with concentric circular blood flow paths connected by gates should have high oxygen transfer efficiency created by secondary flows inherent in the design, and CO_2 clearance should be optimized with very short fibers. To test this hypothesis a membrane lung was designed and fabricated and referred to as the M-Lung.

Methods

The M-Lung design is shown in Fig. 1. The device has an outer shell comprising a blood inlet, blood outlet, gas inlet, and gas outlet ports, as shown in Fig. 1A. This outer shell encloses a fiber bundle separated into compartments radially by concentric, circular dividers. Each divider has a gate opening, allowing the blood to flow through the fiber bundle compartments; the blood from the blood inlet port flows through the fiber bundle compartments into the lumen of the blood outlet port. The fiber bundle (Fig. 1A,B) comprises an array of microporous hollow fibers with the upper and lower ends potted, so the interior lumens of the fibers communicate with plenum between the gas ports and the fiber bundle. The fiber bundle is wound around the concentric dividers such that the main direction of blood flow is perpendicular to the direction of gas flow (Fig. 1B). The specifications for the initial lung design were intended for testing in our model of end stage lung disease (ESLD)[9] driven by arterial blood pressure without a pump.[10] These specifications are: fiber length 2 cm, device diameter 10 cm, rated flow ≥1 L/min, oxygen transfer at rated flow ≥50 mL/min, pressure drop at 1L/min of 60 mmHg, and CO_2 clearance that is four times oxygen transfer. A membrane lung with these specifications would provide total gas exchange for a 10 kg child and total systemic CO_2 removal for an adult. Computational fluid dynamics (CFD) and particle image velocimetry (PIV) based modeling defined the prototype design for testing. The following parameters were evaluated: rated flow, surface area, oxygen transfer efficiency, priming volume, transit time, pressure drop, and CO_2 clearance within the size properties.

CFD Design

In order to evaluate and optimize flow patterns through the M-Lung housing, the flow through the M-Lung housing was simulated both with and without the fiber bundle.

Author Manuscript Author Manuscript Author Manuscript Author Manuscript

SolidWorks (Dassault Systèmes SolidWorks Corp., Concord, MA) and Creo (PTC Inc., Needham, MA) computer-aided design (CAD) software was used to create each model, which was then imported into the COMSOL Multiphysics (COMSOL AB, Stockholm, Sweden) CFD software program. Blood was modeled as an incompressible Newtonian fluid, with a density of 1060 kg/m^3 and dynamic viscosity of 0.003 Pa s. The boundary conditions were set as follows: wall=no slip, inlet=pulsatile flow (frequency=1 Hz, amplitude=2×average flow rate, waveform=sinusoidal), and outlet=atmospheric pressure. Representative CFD profiles are shown in Fig. 2.

A finite element formulation based on the Galerkin method was used to solve for the governing equations. Convergence criteria were defined. The velocity and pressure of the flow were found directly using the software. The hollow membrane fiber bundle was incorporated into our model as a porous media, governed by Darcy's law with the Brinkman and Forchheimer extensions.[11,12] The volume of the solid fiber bundle was determined by equation 1. The porosity was determined by equation 2. The surface area was determined by equation 3. The permeability was determined by equation 4.[13–16]

$$V_{\text{fiber bundle}} = \pi r_{\text{HFM}}^2 H N_{\text{HFM}} \quad \text{Eq 1}$$

$$\delta\dot{\text{I}}\text{IJ}\acute{\text{U}}_P = \frac{V_{\text{fiber bundle}} - V_{\text{fibers}}}{V_{\text{fiber bundle}}} \quad \text{Eq 2}$$

$$A_{\text{fibers}} = \pi d_{\text{HFM}} H N_{\text{HFM}} \quad \text{Eq 3}$$

$$\kappa = \frac{\delta\dot{\text{I}}\text{IJ}\acute{\text{U}}_P^{\,3} d_p^{\,2}}{150(1 - \delta\dot{\text{I}}\text{IJ}\acute{\text{U}}_P)^2} \quad \text{Eq 4}$$

In the above equations, d_{HFM} denotes the fiber membrane outer diameter, N_{fiber} is total number of fibers, r is the radius of each fiber. H is the height of the fibers, and ϵ_P is the porosity of the fiber bundle. Note that the porosity is the ratio of the space in the fiber bundle occupied by blood to the total volume of the fiber bundle (blood and fibers). The total priming volume is not used because that value includes areas in the device not occupied by the fiber bundle, such as the inlet/outlet and the blood gates. The effective particle diameter, d_p, is estimated as 1.5 times the fiber membrane outside diameter.[16]

The effects of varying the fiber bundle density was studied by varying the permeability, κ (m^2) of the porous medium

Author Manuscript Author Manuscript Author Manuscript Author Manuscript

PIV Testing

In order to verify simulated flow patterns through the M-Lung housing, optical visualization of flow patterns through the M-Lung were carried out using particle image velocimetry (PIV). The experimental setup is shown in Fig. 3A. The M-Lung prototype comprised a poly(methyl methacrylate) (PMMA) housing. Deionized water was used as the model fluid to represent the blood in these preliminary experiments, since water provided sufficient optical clarity for the particle velocimetry measurements described below. With blood, particle velocity and secondary flows are expected to be reduced slightly due to increased viscosity. Fluid through the M-Lung was pumped using a peristaltic pump set to flow rates of 1.5 L/min and 3.0 L/min to match the inlet flow rates used in CFD simulations. The water was seeded with neutrally buoyant microporous round polyamide seeding particles (diameter=20 μm, density=1.03 g/m^3, Dantec Dynamics Co., Skovlunde, Denmark). These particles were illuminated by a pulsed Nd-YAG laser light (Model: Solo III 15Hz, No: 16155, wavelength 532 nm, New Wave Inc., Fremont, CA, U.S.) as shown in Fig. 3B. The laser's beam passed through a cylindrical lens (Modular Focus, f=-6mm, Rodenstock Co., Munich, Germany) and then shaped into a laser light sheet (<1 mm thickness and 100 mm in width) that illuminated the area of interest. The images were captured by a CCD camera (Flowmaster 3S. resolution: 1280x1024 pixels, LaVision Inc., Goettingen, Germany), which was positioned as shown in Fig. 3A. Successive pairs of single exposed images were then processed employing PIV software (Davis 6.2, LaVision Inc., Goettingen, Germany). Each of the images was divided into small interrogation areas of 32x32 pixels, and was cross correlated with each other with a 50% overlap. A time sequence of the velocity field was obtained by capturing successive pairs of images and repeating the image cross correlations. The experimental velocity field images were then compared with previously obtained computational velocity fields through the M-Lung housing (without fibers).

Prototype Fabrication and In vitro Testing

In order to evaluate the blood gas exchange performance of the M-Lung, functional prototypes, shown in Fig. 4, were fabricated as follows: The M-Lung housing was manufactured using stereolithography (Objet Eden 350v, material: photopolymer "Full Cure 720"), and the fiber bundle comprised a cross-wound mat (Fig. 4A) of hollow microporous polypropylene (PP) membrane fibers (Membrana GmbH, Wuppertal, Germany; diameter 380 μm with 17 fibers/cm), wrapped tightly resulting in a fiber bundle porosity of 0.58, permeability $1.93*10^{-9}$ m^2, fiber surface area of 0.28 m^2, fiber length of 2 cm, and total priming volume of 47 mL. As potting material, a biocompatible, addition-curing silicone rubber (Wacker Chemie AG, Munich, Germany) was utilized, as shown in Fig. 4B. 4C.

The functional performance of the M-Lung was evaluated in vitro using a test circuit in accordance with the Food and Drug Administration Guidance for Cardiopulmonary Bypass Oxygenators 510(k) guidelines.[17] Fresh bovine blood was anticoagulated with heparin to obtain an activated clotting time (ACT) > 480 s and filtered through a 70–120 μm screen filter into a clean carboy. The circuit was primed and deaired using a 0.9% sodium chloride (saline) solution, which was displaced by filtered blood from the filtration reservoir. The circuit total hemoglobin was measured and adjusted with saline solution to 12 ± 1 g/dL. Gas lines from the three gas flow controllers (O_2, N_2, and CO_2) were connected to the

Author Manuscript Author Manuscript Author Manuscript Author Manuscript

conditioning device (Novalung iLA, Xenios AG, Heilbronn, Germany), and the overall gas mixture was controlled by controlling the flow rate of these individual gases during the conditioning process. A flow probe (Transonic, Ithaca, NY) was used to monitor and control the blood flow rate through the circuit, while pressure transducers were connected to the blood inlet and blood outlet sites of the test device to monitor the pressure drop across the M-Lung. A heat exchanger connected to the circuit was used to warm circuit blood to 37 ± 1 ºC. The blood was pumped and recirculated through the conditioning device until the blood pool reached venous conditions, as outlined in Fig. 5 and Table I. The conditioned blood flow was then directed to the test device alone, and the outflow of the test device was directed to the second carboy, comprising a single pass test. The test device was ventilated using a sweep gas comprised of 100% O_2.

The performance of the M-Lung was evaluated over a range of inlet blood flow rate (Q_b) and sweep gas flow rates (Q_g). For each combination of Q_b and Q_g, a blood inlet, blood outlet, and gas outlet sample were obtained, and the inlet and outlet blood pressures were recorded. Between test intervals, the test device was flushed with 100% O_2 to prevent water condensation in the gas phase compartment of the test device. All samples were analyzed using a blood gas analyzer (ABL 800 Flex, Radiometer, Copenhagen, Denmark). The rated flow was determined as the maximum flow at which the test device outlet hemoglobin O_2 saturation was ≥95%. The O_2 transfer rate (VO_2, mL/min) at rated flow was calculated as shown in Eq. 5–7.[6,18]

$$C_{oxy}=13.4 \bullet tHb \bullet \frac{\%SAT}{100}+0.0314 \bullet pO_2 \qquad pO_2=\frac{-19.7}{\left(\frac{\%SAT}{100}-1.21\right)} \quad (4,5)$$

$$VO_2=Q_b \bullet [C_{oxy-post}-C_{oxy-pre}] \quad (6)$$

Where C_{oxy} = O_2 concentration in blood ($mL_{O2}\ L_{blood}^{-1}$), tHb = hemoglobin concentration ($g\ dL^{-1}$), %SAT = hemoglobin O_2 saturation (%), Q_b = blood flow rate (L/min); $C_{oxy-post}$= post-oxygenator O_2 concentration ($mL_{O2}\ L_{blood}^{-1}$), and $C_{oxy-pre}$= pre-oxygenator O_2 concentration ($mL_{O2}\ L_{blood}^{-1}$). The CO_2 transfer rate (VCO_2, mL/min) was calculated as given in Eq. 7:

$$VCO_2=\triangle CO_2 \bullet F \bullet 1000 \quad (7)$$

Where ΔCO_2 = % CO_2 in the outlet gas sample and F = sweep gas flow (L/min). The error bars denote the standard error of mean for each measurement.

Results

The CFD results, as shown in Fig. 2 show a well-distributed blood flow profile through the device with minimal regions of low blood flow. The results further demonstrate the

Author Manuscript Author Manuscript Author Manuscript Author Manuscript

formation of transient flow vortices through the M-Lung housing. These vortices are dampened by the membrane fiber bundle, with the magnitude of dampening dependent on the permeability of the membrane fiber bundle (Fig. 2B).

A comparison of the flow through the M-Lung obtained using simulations and optical flow visualization is shown in Fig. 3B. The PIV results demonstrate similar flow patterns to those obtained computationally; after the fluid passes through the gate of the concentric divider.

In in vitro studies, the M-Lung prototype (Fig. 6A), comprising a fiber bundle surface area of 0.28 m^2 and priming volume of 47 ml, demonstrated a rated flow of 2.0 L/min (Fig. 6B). Further, the device was able to remove 200 mL/min of CO_2 at rated flow using a sweep gas of 16.0 L/min (Fig. 6C). The transit time at rated flow is 1.8 seconds (47 cc volume at 2000 cc/minute).

The blood-side pressure drop across the device comprising a fiber bundle of porosity = 0.59 was 49 mmHg and 106 mmHg at blood flow rates of 1.0 and 2.0 L/min, respectively (Fig. 7). This pressure drop was within the specifications designed for 1 L/min blood flow and pressure drop 60 mmHg. The highest shear forces generated within the housing are 30 dyne/cm^2.

The permeability and porosity of the fiber bundle can be modulated in the fabrication process by varying the number of fibers/cm and/or the spacing between each layer of fibers. The relationship between fiber bundle permeability and simulated M-Lung pressure drop, priming volume, and fiber surface area is shown in Fig. 8A-C. The simulations demonstrate that looser wrapping (or fewer fibers per mat) would result in increased porosity and permeability accompanied by significant reduction in the pressure (Fig. 8A). This would result in larger calculated void volume (Fig. 8B).and lower surface area (Fig. 8C) resulting in less oxygen transfer per square meter.

Discussion

The key to maximize oxygen transfer per surface area in membrane lungs is mixing, and thereby disrupting the diffusion boundary layer, through an increase in vorticity and secondary flows.[2] Flow through circular paths will induce secondary flows to create mixing, yet a long circular spiral has high resistance. Concentric circles connected by gates created secondary flows without increasing resistance. Intense vortices are created within the blood path (Fig. 2), but these vortices are dampened by the fiber bundle. Significant mixing also occurs as blood passes through the gates. The net result of the mixing on oxygenation manifested as efficiency of oxygenation per surface area and as rated flow. In vitro studies demonstrate highly efficient gas exchange within the M-Lung; the prototype maintained an outlet oxygen saturation of ≥95% for blood flow rates up to 2.0 L/min with a fiber bundle surface area of 0.28 m^2 and priming volume of 47 ml. The rated flow of the prototype was twice the goal in our specifications. Several similar size devices are compared in Table II. The oxygen transfer efficiency (mL_{O2}/m^2 min^{-1}) of the M-Lung prototype is 357 mL_{O2}/m^2 min^{-1}. The oxygen transfer efficiency of similar commercial devices with predominantly straight flow path is 128–204 mL_{O2}/m^2 min^{-1}. The experimental Pedipump lung has a single

Author Manuscript Author Manuscript Author Manuscript Author Manuscript

circular chamber and blood is driven by an integral centrifugal pump.[19] The oxygen transfer efficiency is 400 cc/m2/min.

The CFD results show a well-distributed blood flow profile through the M-Lung with minimal regions of low blood flow. The results also demonstrate the formation of transient flow vortices through the M-Lung housing, suggesting that the gated design promotes passive secondary flow mixing. This mixing is dampened by the membrane fiber bundle, with the magnitude of dampening dependent on the permeability of the membrane fiber bundle. The simulations demonstrate that an increase in secondary flow mixing and a significant reduction in the pressure drop across the M-Lung could be achieved by increasing the fiber bundle permeability. The specific pattern of secondary flows generated depends on a variety of factors, including inlet flow rate and pulsatility and specific configuration of dividers and gates. Since the inlet flow rate and pulsatility are dependent on the perfusion system (pump or native circulation), variations of this design will incorporate a variety of divider and gate configurations to meet different specifications.

Despite its low priming volume and efficient gas exchange, the M-Lung maintains a sufficiently low blood-side pressure drop across the relevant range of blood flow rates. At a blood flow rate of 1.0 L/min, the M-Lung had a blood-side pressure drop <50 mmHg, which is within the range supported by a systemic arteriovenous pressure gradient for the intended application of CO_2 removal. At its rated flow of 2.0 L/min, the M-Lung prototype had a pressure drop of 106 mmHg, which is acceptable but very high for pump perfusion, and too high for pulmonary artery perfusion,

The pressure drop can be regulated to any desired level by changing the density of fibers (porosity or permeability) and the size of the device, which we will do for other prototypes depending on the driving pressure source. These relationships simulated by CFD are shown in Fig. 8.

We did not test hemolysis, thrombogenicity, or durability because the housing components were fabricated by 3D printing which creates a rough surface. The next prototypes will be injection molded or machined, creating a very smooth surface for durability and blood damage testing.

The prototype was able to remove 200 mL/min of CO_2 at the rated flow and gas to blood flow ratio of 16:1. The CO_2 clearance is largely dependent on the sweep gas flow rate to blood flow rate ratio and can be further increased by increasing the sweep gas flow. The relatively short gas exchange fibers allow the M-Lung to maintain a sufficiently low gas side pressure drop at higher sweep flows and minimize water accumulation in gas phase enhancing the CO_2 removal efficiency/capacity of the device. Testing of the durability of CO_2 clearance awaits prolonged animal trials.

This M-Lung design meets the functional requirements for providing CO_2 removal for adults and total respiratory support for infants and small children (with a pump). In addition to sufficient gas transfer, it comprises a low priming volume, allowing for minimal hemodilution and rapid transit time. The rapid transit time at rated flow and the absence of corners where blood can stagnate should minimize thrombogenicity. Thrombogenicity and

Author Manuscript Author Manuscript Author Manuscript Author Manuscript

anticoagulant requirements will be assessed in chronic animal trials. Hemolysis testing will be done in vitro and in vivo using devices with smooth blood contact surfaces.

We intentionally began these studies with a small membrane lung design. Given its compact size, controllable resistance, and potential for low thrombogenicity, this size M-Lung has potential for providing long-term ambulatory respiratory support, in arteriovenous mode for clearance of CO_2 for patients with end-stage COPD, or (at higher porosity) pulmonary artery to left atrium mode for total lung support in children. The design could be scaled up to achieve total adult respiratory support (ie. a rated flow of 5 L/min). Scaling up to adult size devices will be done with a return to CFD and PIV to optimize the properties of a device with a 5 L/min rated flow, pressure drop <120 mmHg at rated flow, and CO_2 transfer 2 times oxygen transfer at rated flow. This would require 0.6 to 0.8 m^2 of gas transfer surface, in contrast with current contemporary adult devices, which comprise 1.5–1.8 m^2.

Conclusions

In conclusion, using CFD and optical flow visualization methods, a unique hollow fiber membrane lung has been designed based on concentric circular blood flow paths connected by gates. In prototype testing, flow patterns and pressure drop across the M-Lung device matched those predicted by CFD. The prototype M-lung has a rated flow of 2 L/min with a fiber surface area of 0.28 m^2, and the oxygenation efficiency is 357 mL/min/m^2. The CO_2 clearance of the M-lung is 200 mL/min at the rated blood flow. Future work will evaluate the performance of the M-Lung in in vivo to further assess its biocompatibility and chronic performance.

Acknowledgments

Source of Funding: NIH 2R01 HD015424-29

Funded in part by the Excellence Initiative of the German federal and state governments in the framework of the I^3TM Seed Fund Program.

References

1. Peirce EC, Dibelius NR. Membrane Lung - Studies with a New High Permeability Co-Polymer Membrane. Trans Am Soc Artif Intern Organs. 1968; 14:220–226. [PubMed: 5701534]
2. Zwischenberger JB, Anderson CM, Cook KE, Lick SD, Mockros LF, Bartlett RH. Development of an implantable artificial lung: challenges and progress. ASAIO J. 2001; 47:316–320. [PubMed: 11482477]
3. Stanzel RD, Henderson M. Clinical evaluation of contemporary oxygenators. Perfusion. 2016; 31:15–25. [PubMed: 26407816]
4. Bartlett RH, Kittredge D, Noyes BS, Willard RH, Drinker PA. Development of a membrane oxygenator-overcoming blood diffusion limitation. J Thorac Cardiovasc Surg. 1969; 58:795–800. [PubMed: 5353670]
5. Drinker PA, Bartlett RH, Bialer RM, Noyes BS Jr. Augmentation of membrane gas transfer by induced secondary flows. Surgery. 1969; 66:775–81. [PubMed: 5822769]
6. Benn JA, Drinker PA, Mikic B, Shults MC, Lacava EJ, Kopf GS, et al. Predictive correlation of oxygen and carbon dioxide transfer in a blood oxygenator with induced secondary flows. Trans Am Soc Artif Intern Organs. 1971; 17:317–322. [PubMed: 5158112]
7. Berger SA, Talbot L, Yao LS. Flow in curved pipes. Ann Rev Fluid Mech. 1983; 15:461–512.

Author Manuscript Author Manuscript Author Manuscript Author Manuscript

8. Nandakumar K, Masliyah JH. Bifurcation in steady laminar-flow through curved tubes. J Fluid Mech. 1982; 119:475–590.
9. Witer LJ, Howard RA, Trahanas JM, Bryner BS, Alghanem F, Hoffman HR, et al. Large animal model of pumpless arteriovenous extracorporeal CO_2 removal using Room air via subclavian vessels. ASAIO J. 2016; 62:110–113. [PubMed: 26461241]
10. Alghanem F, Bryner BS, Jahangir EM, Fernando UP, Trahanas JM, Hoffman HR, et al. Pediatric artificial lung: A low-resistance pumpless artificial lung alleviates an acute lamb model of increased right ventricle afterload. ASAIO J. 2017; 63:223–228. [PubMed: 27861431]
11. Amiri A, Vafai K. Transient analysis of incompressible flow through a packed bed. Int J Heat Mass Tran. 1998; 41:4259–4279.
12. Ergun S. Fluid flow through packed columns. Chem Eng Prog. 1952; 48:89–94.
13. Khanafer K, Cook K, Marafie A. The role of porous media in modeling fluid flow within hollow fiber membranes of the total artificial lung. J Porous Media. 2012; 15:113–122. [PubMed: 23471191]
14. Vafai K. Convective flow and heat-transfer in variable-porosity media. J Fluid Mech. 1984; 147:233–259.
15. Vafai K. Analysis of the channeling effect in variable porosity media. J Energ Resour-Asme. 1986; 108:131–9.
16. Pacella HE, Eash HJ, Federspiel WJ. Darcy permeability of hollow fiber bundles used in blood oxygenation devices. J Memb Sci. 2011; 382:238–242. [PubMed: 22927706]
17. [cited October 1, 2016] Guidance for Cardiopulmonary Bypass Oxygenators 510(k) Submissions; Final Guidance for Industry and FDA Staff [Internet]. Food and Drug Administration. 2000. Available from: http://www.fda.gov/MedicalDevices/DeviceRegulationandGuidance/GuidanceDocuments/ucm073668.htm
18. Bartlett RH. Physiology of gas exchange during ECMO for respiratory failure. J Intensive Care Med. 2017; 32:243–248. [PubMed: 27040797]
19. Wu ZJ, Gellman B, Zhang T, TAskin E, Dasse KA, Griffith BP. Computational fluid dynamics and experimental characterization of the Pediatric Pump-Lung. Cardiovasc Eng Tech. 2011; 2:276–287.

Author Manuscript
Author Manuscript
Author Manuscript
Author Manuscript

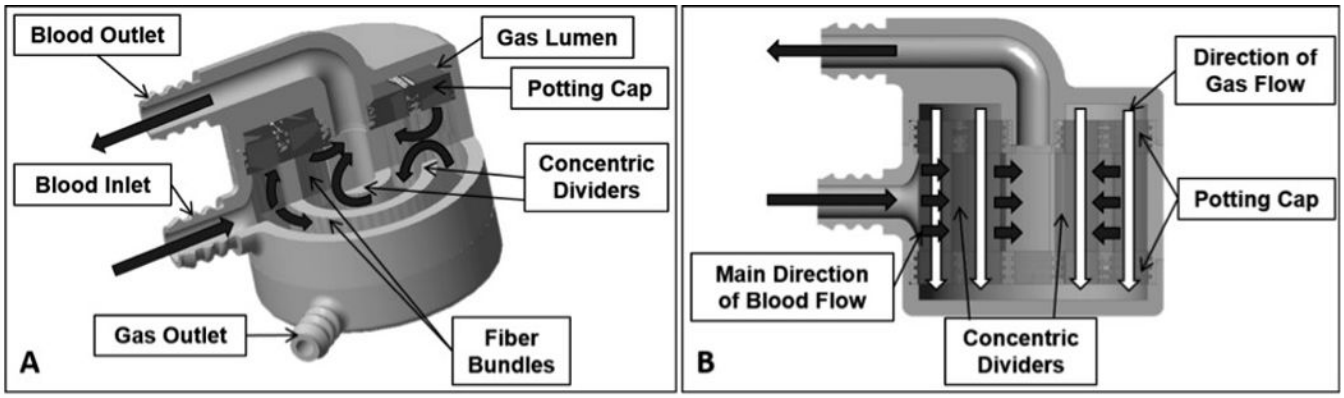

Figure 1. M-Lung design

Cross sectional views of the assembled device are shown in (A) and (B). The black and white arrows indicate the main direction of blood flow and gas flow, respectively.

Author Manuscript Author Manuscript Author Manuscript Author Manuscript

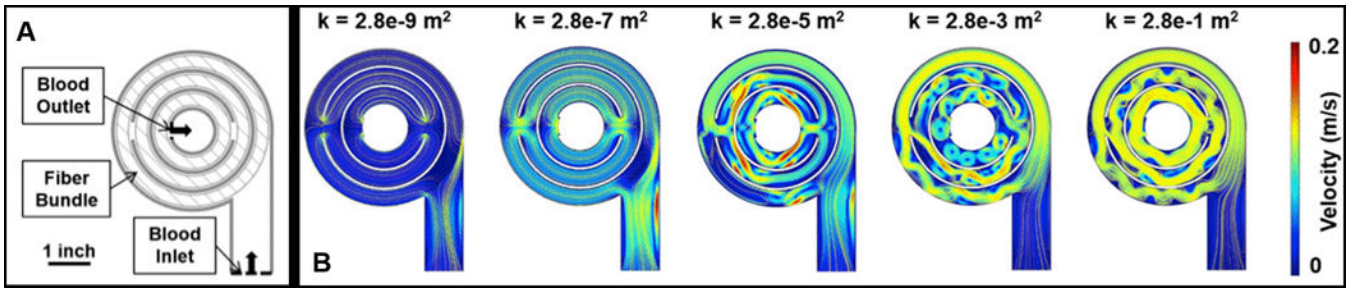

Figure 2. Computational fluid dynamics flow

(A) shows the simulated 2-D profile of the M-Lung, while (B) shows the velocity profiles obtained at the trough of the inlet pulse for varying fiber bundle permeability (k). The yellow lines denote velocity streamlines.

Author Manuscript Author Manuscript Author Manuscript Author Manuscript

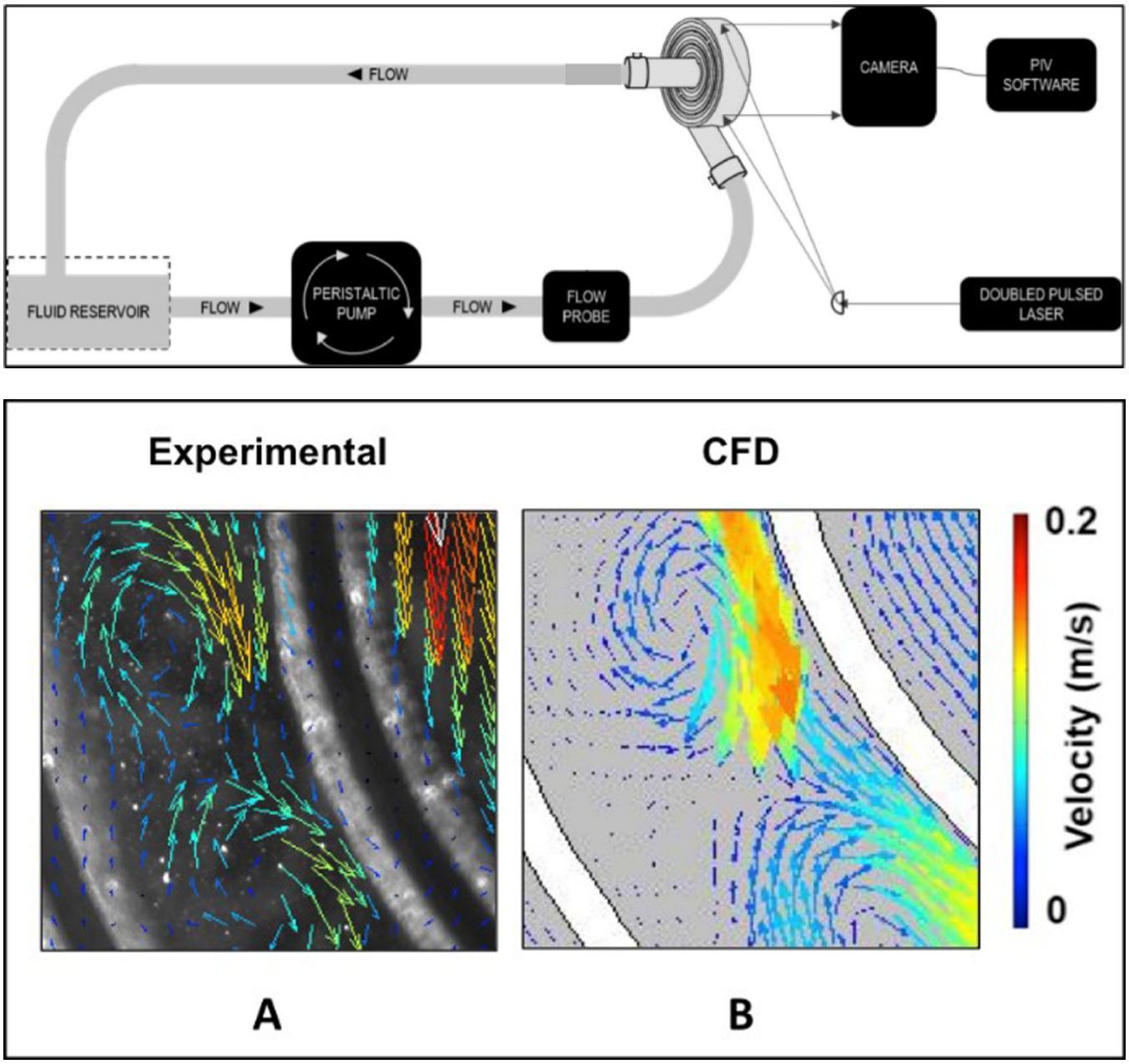

Figure 3.

(A) **Particle image velocimetry setup.** The grey arrows indicate the laser path, which originates from the laser source, is shaped into a laser sheet through a cylindrical lens, and illuminates a slice of the M-Lung device. (B) **Comparison of simulated and experimental flow through the M-Lung housing.** The experimental PIV results (A) demonstrate similar flow patterns to those obtained computationally (B).

Author Manuscript Author Manuscript Author Manuscript Author Manuscript

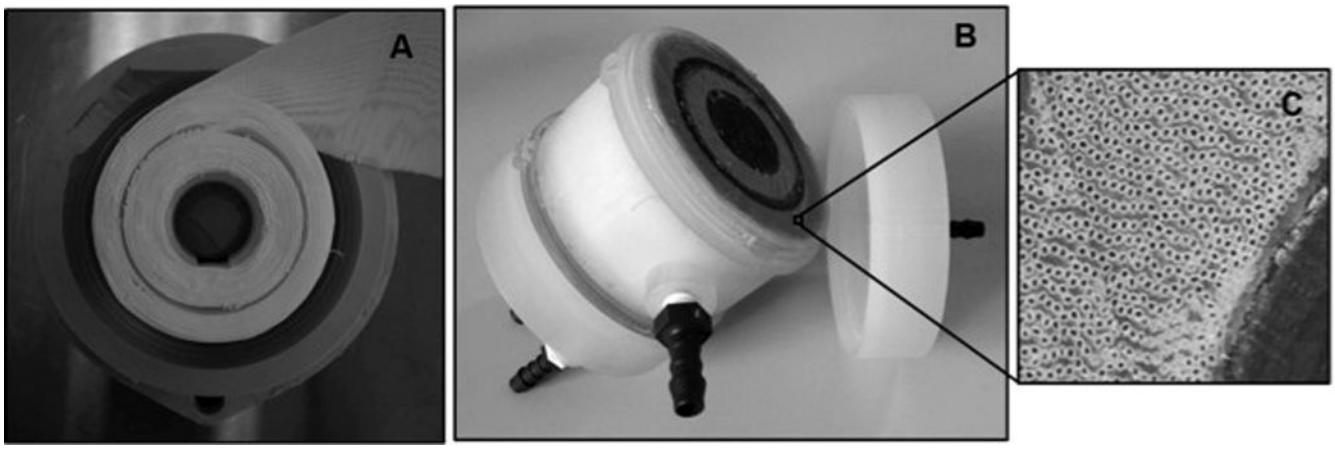

Figure 4. Manufacturing functional M-Lung prototypes

(A) shows the fiber mat wound with the divider in place, while (B) shows the assembled device. A zoomed-in view of the patent, potted fibers is given in (C).

Author Manuscript Author Manuscript Author Manuscript Author Manuscript

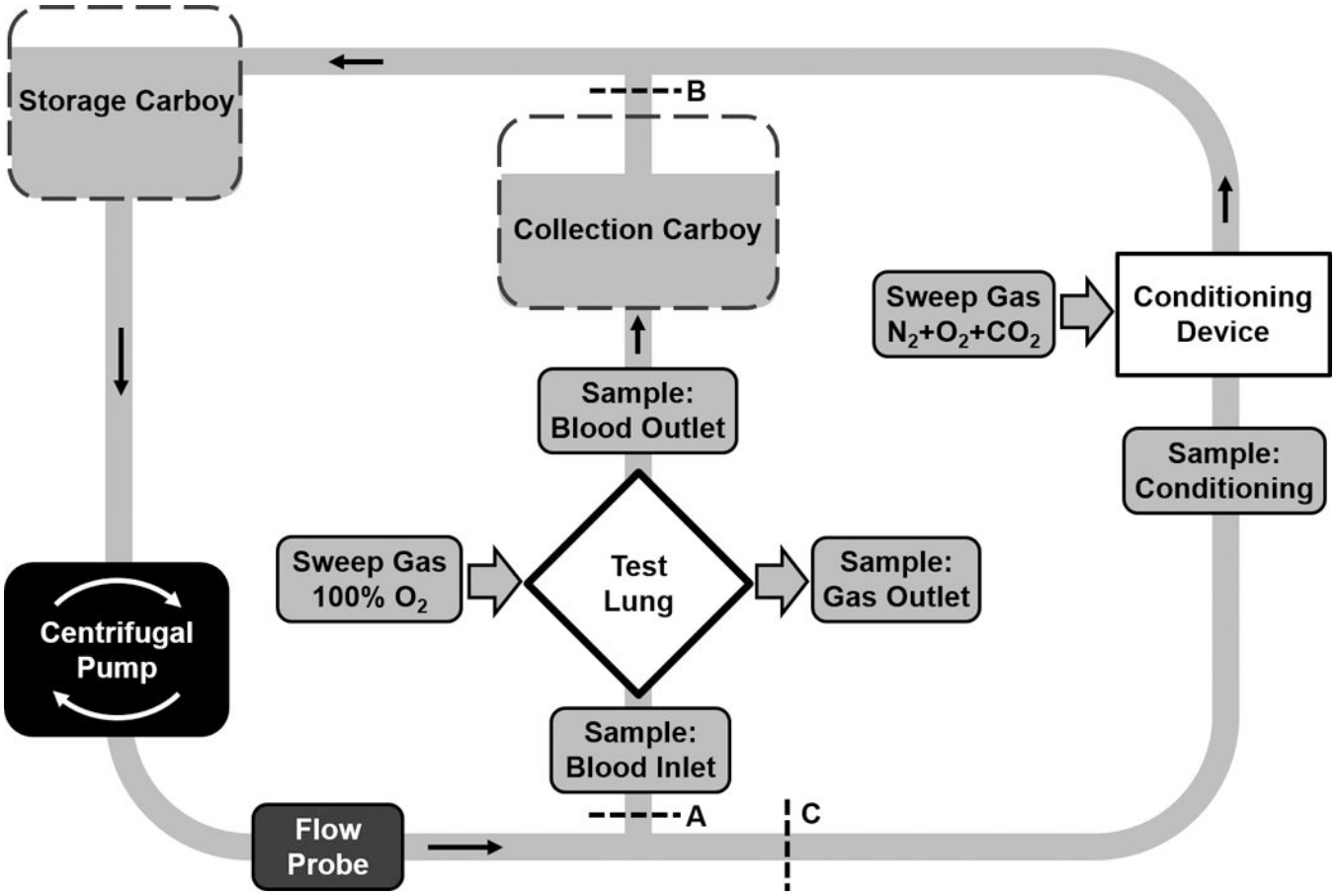

Figure 5. The in vitro test system

Blood is circulated through the conditioning lung until venous conditions are stable (A and B clamped). Then flow is diverted through the M-Lung at specified flow as a single pass and gas transfer measurements are made (C clamped, A and B open).

Author Manuscript Author Manuscript Author Manuscript Author Manuscript

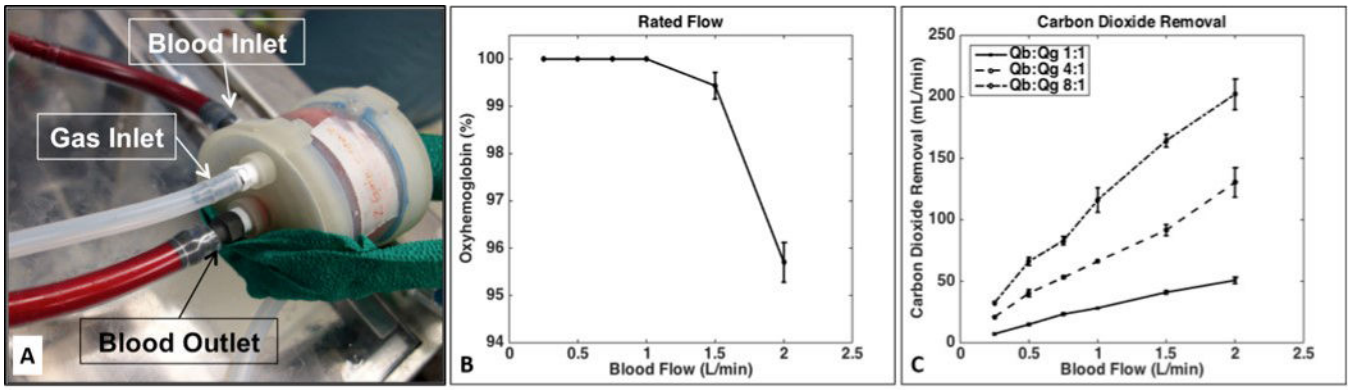

Figure 6. M-Lung in vitro gas exchange performance

The M-Lung, shown in (A), has a rated flow of 2.0 L/min (B) and a CO_2 clearance of 200 mL/min at the rated flow (C).

Author Manuscript Author Manuscript Author Manuscript Author Manuscript

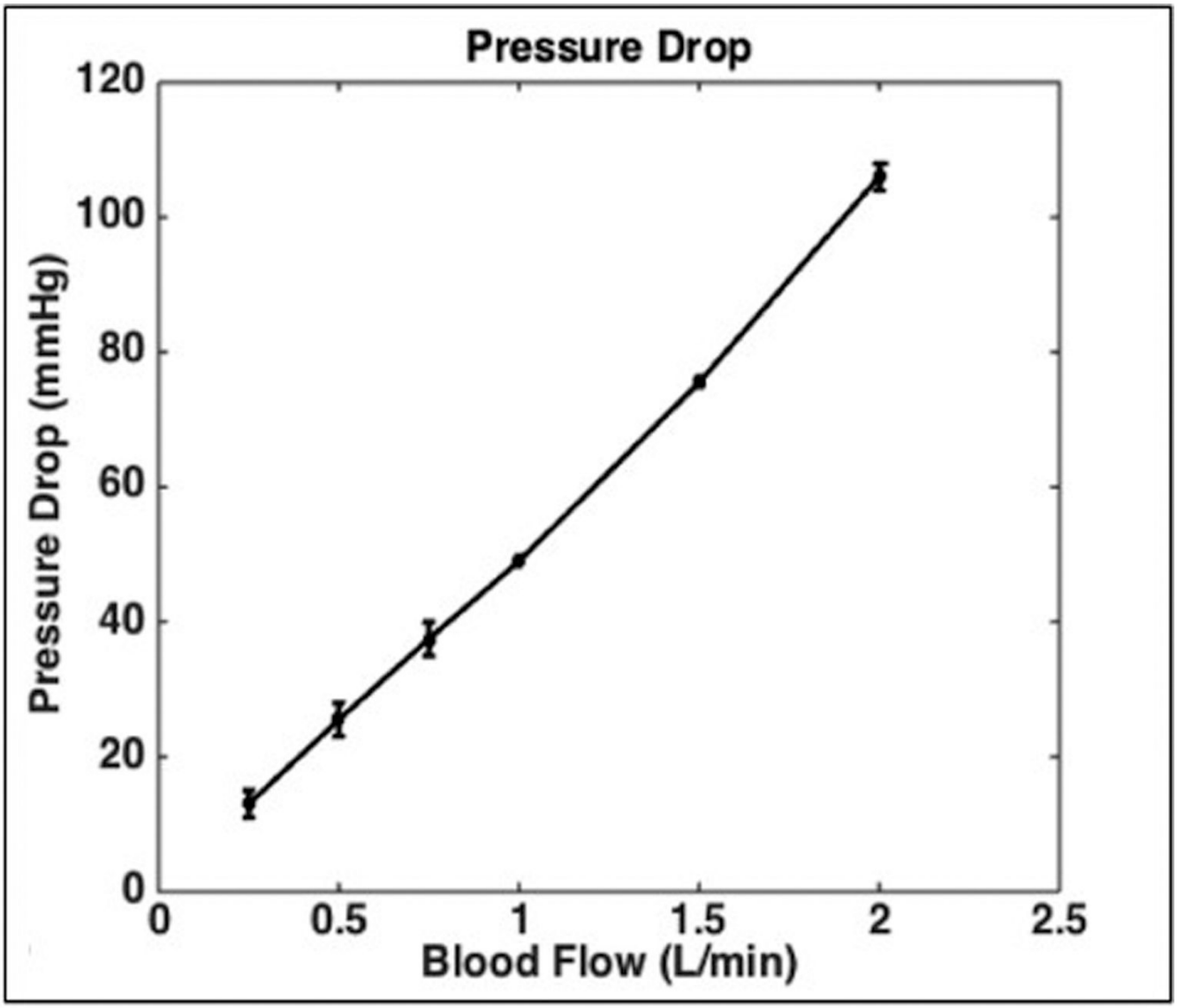

Figure 7. M-Lung in vitro pressure drop

The M-Lung demonstrates a pressure drop of 49 mmHg at 1.0 L/min with a fiber bundle porosity of 0.59.

Author Manuscript Author Manuscript Author Manuscript Author Manuscript

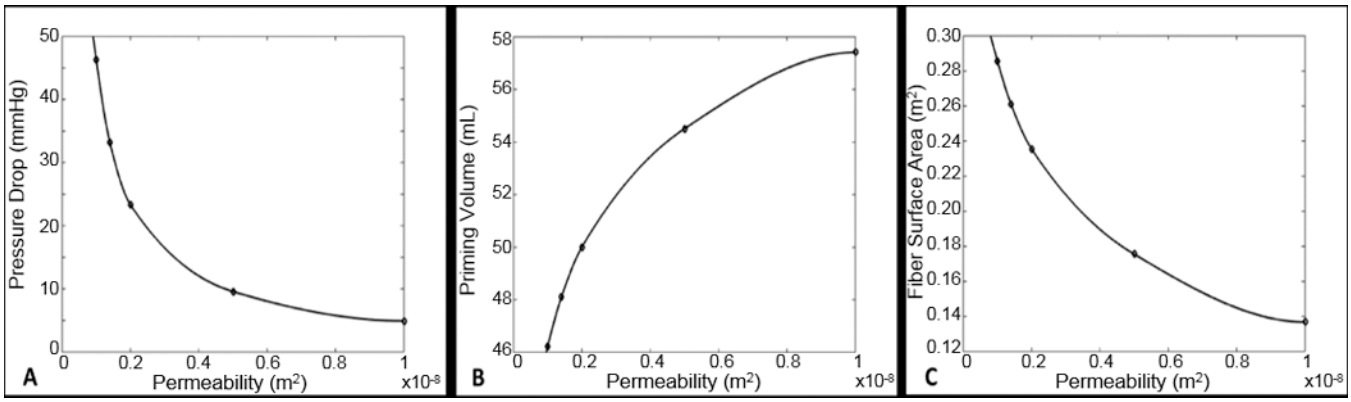

Figure 8.

Simulated effects of varying fiber bundle permeability on M-Lung pressure drop for Q_b = 0.5 L/min (A), priming volume (B), and fiber surface area (C). The prototype has a permeability of 0.27x10^-8 m^2.

Author Manuscript

Author Manuscript

Author Manuscript

Author Manuscript

Table I

Blood target specifications for in vitro testing

Parameter (Units)	Target Value
Hemoglobin (g dL^{-1})	12±1
O_2 Saturation (%)	65±5
pCO_2 (mmHg)	45±5
Base Excess (mmol L^{-1})	0±5
pH	7.4±0.1
Glucose (mg dL^{-1})	100-300
Activated Clotting Time (s)	>480
Temperature (°C)	37±2

Author Manuscript Author Manuscript Author Manuscript Author Manuscript

Table II

Comparison of similar size membrane lungs

Membrane Lung	Fiber Surface Area (m^2)	Priming Volume (mL)	Maximum or Rated Flow (L/min)	ΔP at Rated Flow* (mmHg)	O_2 Transfer at Rated Flow** (mL_{O2} min^{-1})	O_2 Transfer Efficiency*** (mL_{O2} min^{-1}/m^2)
Terumo Capiox RX05	0.5	43	1.5	110[1]	75	150
Maquet Quadrox-i Neonatal	0.38	40	1.5	58[2]	75	197
Maquet Quadrox-i Pediatric	0.8	99	2.8	60[3]*1.5 L/min	140	175
Medos Hilite 1000	0.39	57	1.0	Data not available	50	128
Medos Hilite 2800	0.8	98	2.8	Data not available	140	175
Sorin Dideco D100	0.22	47	0.7	175	35	159
Sorin Dideco D101	0.61	115	2.5	155	125	204
Pedipump Lung	0.3	110	2.5	150	120	400
M-Lung	0.28	47	2.0	106	100	357

*If ΔP data was not available at rated flow, the flow rate for the ΔP in the table is specified;

**Rated flow is flow of standardized venous blood at which outlet blood oxygen saturation is 95%;

***O_2 transfer efficiency = O_2 transfer at rated flow (mL_{O2} min^{-1}) per fiber surface area (m^2). Data for commercial devices were obtained from manufacturer manuals for each device. Data for the pedipump lung is taken or calculated from reference 19.

[1]J. Dubois, L. Jamaer, U. Mees, J.-L. Pauwels, F. Briers, J. Lehaen, and M. Hendrikx, Perfusion 19, 315 (2004).

[2]R.M. Ginther, R. Gorney, and R. Cruz, Perfusion 28, 194 (2013).

[3]R.K. Mathis, J. Lin, N.M. Dogal, F. Qiu, A. Kunselman, S. Wang, and A. Ündar, Perfusion 27, 470 (2012).

ASAIO J. Author manuscript; available in PMC 2018 September 01.